The effect of oxygen partial pressure and substrate temperature on the structural and optical properties of ZnO nanowires

R. SUBBA REDDY[a,*], S. UTHANNA[a], T. SRIKANTH[b], A. SIVASANKAR REDDY[b], B. RADHA KRISHNA[c]
[a]*Department of Physics, Sri Venkateswara University, Tirupati-517 502, India*
[b]*Department of Physics, Vikrama Simhapuri Univerisity PG Center, Kavli-524 021, India*
[c]*Department of Physics, NBKR Institute of Science and Technology, Vidyanagar-524413, India*

In this paper ZnO thin films were prepared by radio frequency reactive magnetron sputtering on p-type silicon (100) and glass substrates by varying the different substrate temperatures and different oxygen partial pressure and study the structural, compositional, microstructrue, morphological and optical properties by X-ray diffraction, scanning electron microscopy, atomic microscopy and UV-Vis-NIR spectrophotometer. The X- Ray diffraction results confirmed that the films consists of ZnO peaks of (100), (002) and (110). The Fourier transform infrared spectrum confirms the presence of Zn-O bonding at wave number of 413 cm^{-1}. The SEM analysis confirms that the films formed at oxygen partial pressure of $8x10^{-3}$ Pa, the nanowires were formed parallel to the surface layer and the nanotubes were formed perpendicular to the surface of the film. The optical transmittance data reveals the average transmittance in the visible range more than 84 % for all the films. The optical band gap of ZnO films increased from 3.04 to 3.14 eV with increase of oxygen partial pressures.

(Received April 13, 2018; accepted February 12, 2019)

Keywords: Zinc oxide, Sputtering, Nanostructure, Nanowires, Optical properties

1. Introduction

Zinc oxide (ZnO) has wide band gap of 3.37 eV and large exiton binding energy of 60 meV at room temperature [1]. ZnO thin films have been investigated due to their potential applications such as transparent conducting films [2], light emitting diodes, laser systems [3], surface acoustic wave devices, optical device, solar cells and gas sensors [4]. Zinc oxide has received much attention due to its unique electrical and optical properties. ZnO can be obtained in a variety of nanostructures including nanocomb, nanorings, nanoflowers, nanobelts, nanowires and nanosheets under specific growth conditions. ZnO nanostructures have played an attractive role in nanodevices like nanogas sensors because of large surface area: enhance the sensing properties of the gas sensors [5]. ZnO nanowires are believed to be a good candidate for gas sensing applications due to its specific area, fine particle size and the quantum confinement properties [6]. Recently, nanostructure ZnO thin films used as gas sensors due to their chemical stability, non-toxicity and low cost. Thin films of ZnO were prepared using various thin film deposition techniques such as electron beam evaporation technique, plasma enhanced chemical vapor deposition, metal organic chemical vapor deposition, spray pyrolysis, sol- gel method, pulsed laser deposition, laser molecular beam epitaxy, and sputtering techniques [7-15] etc. Among them, one of the most commonly used technique is sputtering method because of simplicity and possibility of obtaining good preferred orientation at low deposition temperatures and uniform film on large area substrates. The properties of sputtered films are highly influenced by the sputter process parameters such as substrate temperature, sputter power, sputter pressure, substrate bias and oxygen flow rate. In this present investigation, nanostructure ZnO thin films were prepared by RF magnetron sputtering technique at different substrate temperatures and oxygen partial pressures and studied the structural, compositional, microstructrue, morphological and optical properties of the as deposited films.

2. Experimentation

2.1. Thin film preparation

ZnO thin films were deposited on silicon and corning glass substrates using RF reactive magnetron sputtering method. Metallic zinc target of 5 cm diameter and 3 mm thick was used for deposition of thin films. The magnetron sputtering system is capable of producing base pressure of $2x10^{-4}$ Pa using diffusion pump and rotary pump combination. The pressure in the chamber was measured with digital Pirani gauge and Penning gauge. The target to substrate distance was kept at 50 mm for all the depositions. The shutter was placed between the target and the substrate in order to prevent the undesirable sputtering.

High purity (99.99%) argon and pure oxygen gases were used as sputter and reactive gases respectively. Before deposition of each film, the Zinc target was pre-sputtered in argon atmosphere for about 10 min in order to remove the surface oxide layer of the target. H. Liu et al. [31] also reported similar experimental conditions in the formation of undoped ZnO thin films. ZnO thin films were deposited on silicon and corning glass substrates at different oxygen partial pressures and substrate tempratures.

2.2. Thin films characterization

The deposited ZnO films thickness measured by using of α- step profilometer. Crystallographic structure, crystallite size and dislocation density of the films were determined with X-ray diffraction (XRD) taken on a Brurker D8 Advance diffractometer at the glancing angle of 4^0 using monochromatic Co $K\alpha_1$ radiation (λ = 1.78897 A^o). Chemical composition of the films was determined by energy dispersive X-ray analysis (EDAX). The microstructure and surface morphology of the films was analyzed by scanning electron microscopy (SEM) and atomic force microscopy (AFM). Fourier transform infrared spectroscopic (FTIR) measurements in the wave number range between 400 and 4000 cm^{-1} were measured using Nicolet Magana IR 750, FTIR spectrometer in order to determine the chemical binding configuration of the deposited films. The optical transmittance was recorded by using Perkin – Elmer UV-Vis-NIR double beam spectrophotometer in the wavelength range of 300 - 2500 nm in order to obtain the optical absorption, optical band gap and refractive index of the films.

3. Results and discussion

3.1. Effect of Substrate temperature

Nanostructure ZnO thin films were deposited on silicon and corning glass substrates by using RF reactive magnetron sputtering at various substrate temperatures in the range 303 to 573 K at optimum oxygen partial pressure of $2x10^{-2}$ Pa. The deposition rate of the films was determined from the thickness and duration of deposition. The deposition rate was influenced by the substrate temperature. The deposition rate first increased from 3.9 to 4.5 nm/min with increase of substrate temperature from 373 to 473 K. On further increasing of substrate temperature to 573 K the deposition rate of the ZnO films decreased to 3.7 nm due to the number of atoms leaving from surface was enhanced by thermal desorption [16].

3.1.1. Structural analysis

Fig. 1 shows XRD profiles of the ZnO films formed at different substrate temperatures. The films formed at substrate temperature of 303 K consists (100), (110) reflections with hexagonal structure of ZnO. As the substrate temperature increased to 373 K, the intensity of (100), (110) reflections decrease and presence of (002) and (101) reflections. The presence of (002) orientation indicated the growth of c- axis orientation. On further increasing of substrate temperature to 473 K the (002) orientation enhanced and remaining peaks are diminished. The enhancement in the c- axis orientation growth with increasing of substrate temperature to 473 K was due to increase in the surface diffusion of absorbed species [17]. As the substrate temperature increases the atoms get sufficient energy and the surface mobility to settle in stable position. This gives rise to the most stable c-axis orientated structure as preferred grown orientation [18]. At higher substrate temperature of 573 K the intensity of c-axis orientation decreased. The decrease of crystallinity at this temperature was due to breaking of the Zn-O bonding and re-evaporating the deposited films rather than enabling the atoms to move to their stable sites.

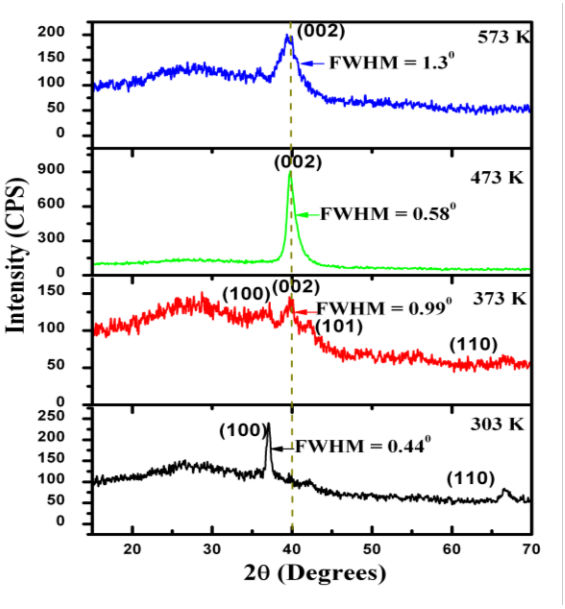

Fig. 1. XRD patterns of ZnO films deposited at various substrate temperatures

The crystalline size of the films was calculated from the Scherrer's formula [19]

$$L = 0.9\ \lambda/\beta\cos\theta \qquad (1)$$

where λ = 1.78897 Å, θ is the Bragg diffraction angle and β is the full width at half maximum (FWHM) of the (002) peak.

The FWHM of (002) peak decreased from 0.99^o to 0.58^o with increase of substrate temperature from 373 to 473 K due to improvement of crystallinity. On further increasing the substrate temperature to 573 K the FWHM increased to 1.3^o. The crystallite size of the ZnO films increased from 9.7 to 16.5 nm with increase of substrate temperature from 373 to 473 K, and it decreased to 7.6 nm at higher substrate temperature of 573 K. It confirmed that the crystalline quality of the ZnO film is better at substrate temperature of 473 K.

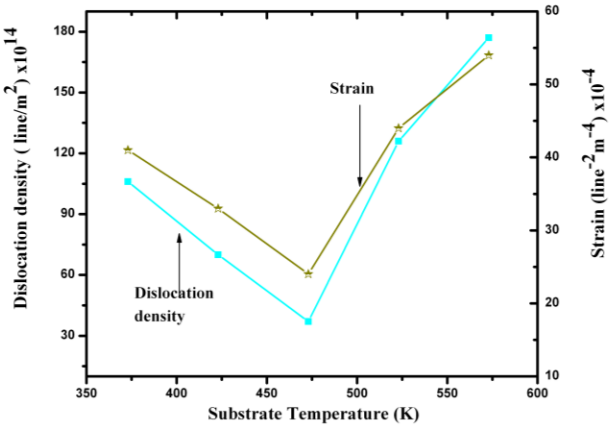

Fig. 2. Variation of dislocation density and strain of ZnO films with substrate temperature

Fig. 2 shows the variation dislocation density, strain of ZnO films at different substrate temperatures. Dislocation density and strain calculated by using below equations [20],

$$\text{Dislocation density}(\delta) = 1/L^2 \quad (2)$$

$$\text{Strain}(\varepsilon) = \beta\cos\theta/4 \quad (3)$$

The dislocation density and strain of the films decreased with increase of substrate temperature from 303 K to 473 K and thereafter it increased at higher substrate temperatures. The strain decreased with increase of substrate temperature due to the mobility of atoms in the films increases with the substrate temperature, which will easy to shift from non-equilibrium position to a more equilibrium position at higher substrate temperatures, thus decrease strain in the ZnO films [21].

3.1.2. SEM analysis

The microstructure images of nanostructure ZnO films deposit at different substrate temperatures on silicon substrates are shown in Fig 3. From the SEM images, the films deposited at room temperature consist small grains with dense surface (Fig.3(a)). As increasing the substrate temperature to 373 K the films consists nanowires with smalls size nanotubes (Fig 3 (b)), and these nanowires formed parallel to the film surface. The similar variation of microstructure was observed in the metal-organic chemical vapour deposited ZnO films by Wu et al. [22]. On further increasing of the substrate temperature to 473 K the nanowires disappeared and hexagonal cone type structure formed due to growing of (002) orientation. At higher substrate temperature provides higher energy for the sputtered particle, enhancing the diffusion and hoping distance the surface gets smooth and grains gets denser.

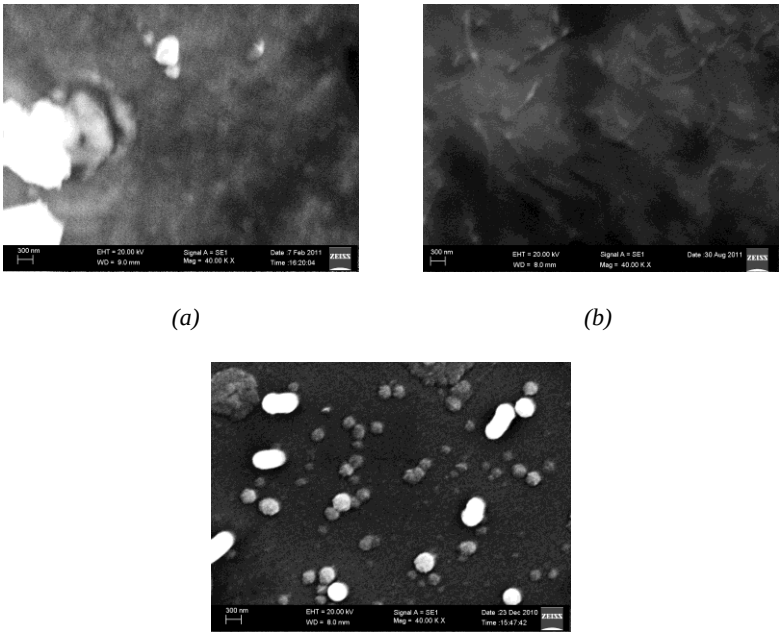

(a) *(b)*

(c)

Fig. 3. SEM images of ZnO films formed at different substrate temperatures: (a) 303 (b) 373 and (c) 473 K

3.1.3. AFM analysis

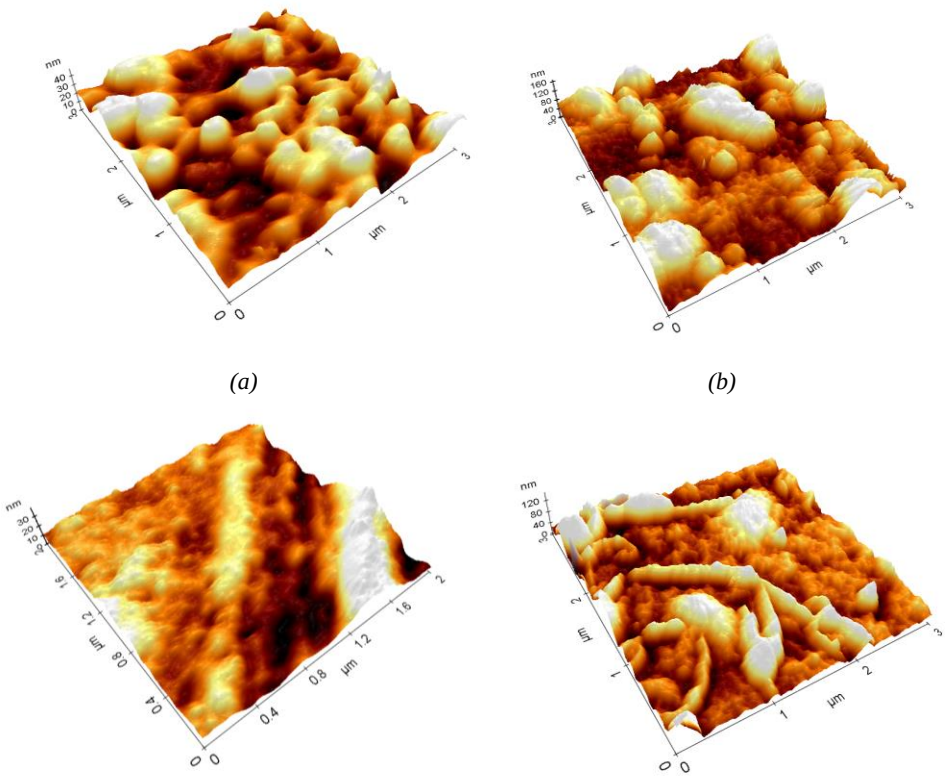

Fig. 4. AFM images of ZnO films formed at different substrate temperatures: (a) 303 (b) 373 (c) 473 and (d) 573 K

Fig. 4 shows the atomic force microscope images of ZnO films at different substrate temperatures. The root-mean-square average (RMS) roughness of the films is 7.3, 25.8, 5.8 and 14.3 nm for 303, 373,473 and 573 K respectively. The low RMS roughness value of 5.8 nm found at substrate temperature of 473 K was due to supply of the excessive thermal energy [23]. In the literature, Zhao et al. [24] reported the RMS roughness increases from 3 to 30 nm with increasing of substrate temperature from 400 to 700 ^{o}C.

3.1.4. FTIR analysis

FTIR spectra of ZnO thin films formed at different substrate temperatures are shown in Fig. 5. The infrared absorption spectra of the ZnO films were recorded in the wavelength 800 – 400 cm^{-1} range. ZnO films formed at substrate temperature of 303 K showed the absorption band at 413 cm^{-1} corresponding to Zn-O stretching vibration with tetrahedral surrounding of Zinc atoms. The absorption peak is shifted to higher wave number side with increase of substrate temperature due to the presence of (002) c-axis orientation. When the substrate temperature increased to 473 K the peak full width at half maximum is decreased due to improving in the crystallinity. Agarwal et al. [25] reported that the FWHM of the Zn-O peak decreased with increasing of substrate temperature due to distribution of vibrational energy becomes narrower, indicating that the deposition method crystallinity of the films is improved with increasing the substrate temperature.

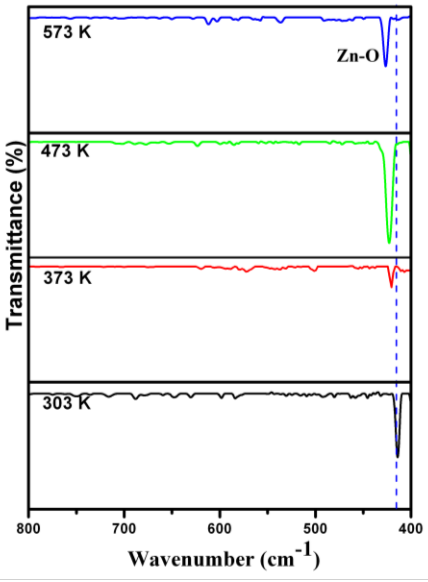

Fig. 5. FTIR spectra of ZnO films formed at different substrate temperatures

3.1.5. Optical properties

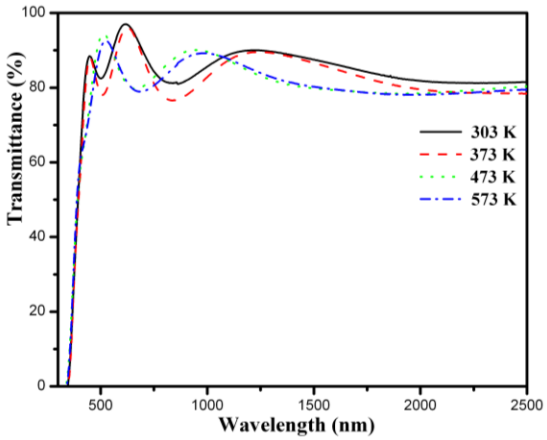

Fig. 6. Optical transmittance spectra of ZnO films formed at different substrate temperatures

Fig. 6 shows the wavelength dependence of optical transmittance spectra of the ZnO thin films deposited at different substrate temperatures. All the films were transparent and average transmittance of the films was about 85 % in the visible wavelength range. It is seen from the spectra that the transmittance of the films decreased with increase of substrate temperature from 303 to 573 K. When the substrate temperature increased the scattering of light is increased, the coherence between the primary light beam and the beams reflected between the films boundary is lost, consequently diminish of the interference fringes and decrease in the transmittance [16]. The fundamental absorption band edge of the films formed at 303 K is about 410 nm. The absorption band edge of the films shifted slightly to the lower wavelength side with the increase of substrate temperature.

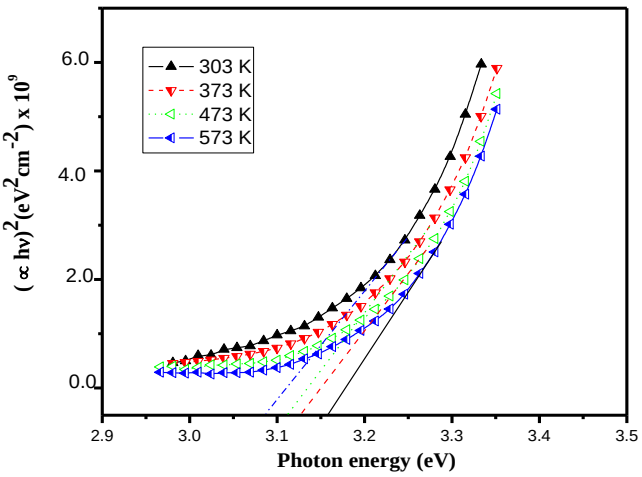

Fig. 7. Plot of (αhv)2 vs hv for ZnO films formed at different substrate temperatures

The optical absorption coefficient (α) was calculated from the relation [26].

$$\alpha=(1/t)\ln(T/(1-R)^2) \quad (4)$$

where T is the transmittance, R is the reflectance and t is the film thickness. The direct band gap was found using the below equation.

$$\alpha h\nu=A(h\nu-Eg)^{1/2} \quad (5)$$

where A is the edge width parameter and Eg the optical band gap. The optical band gap was obtained from the linear portion of the plots of $(\alpha h\nu)^2$ versus hν. The optical band gap decreased from 3.10 to 3.17 eV with increase of substrate temperature from 303 to 573 K. Band gap of undoped ZnO films varies little with Ts varying due to oxygen atoms to jump in to interstitial space, so oxygen vacancies easily form at low Ts and band gap increases with temperature [27]. The decrease of optical transmission and increase of absorption coefficient with the increase in substrate temperature may be due to the presence of oxygen vacancies.

The refractive index (n) of the films was determined from the optical transmittance interference data employing Swanepoel's envelope method [28] using the relation,

$$n(\lambda) = [N + (N^2 - n_0^2 n_1^2)^{1/2}]^{1/2} \quad (6)$$

and

$$N = 2n_0n_1[(T_M-T_m)/T_MT_m] + (n_0^2+n_1^2) \quad (7)$$

where T_M and T_m are the optical transmittance maximum minimum respectively. The refractive index of the films increased from 2.32 to 2.58 with the increase of substrate temperature from 303 to 573 K. As the substrate temperature increased the refractive index of the films increased due to the improvement in the packing density and the polycrystalline nature.

3.2. Effect of oxygen partial pressure at substrate temperature of 523 K

Nanostructure ZnO films deposited on silicon and glass substrates by RF magnetron sputtering at different oxygen partial pressures ranging from $8x10^{-3}$ to $8x10^{-2}$ Pa at substrate temperature of 523 K. The deposition rate of ZnO films decreased from 5.9 to 2.5 nm/min with increases of oxygen partial pressure (Table 1). At higher oxygen partial pressure of $8x10^{-2}$ Pa the deposition rate is low due to oxidation of the target, poison of the target surface. At lower oxygen condition the ratio of high energy argon atoms increases, the inert gas atoms bombardment of the target enhanced, then the releasing number of target atoms increases.

3.2.1. Structural analysis

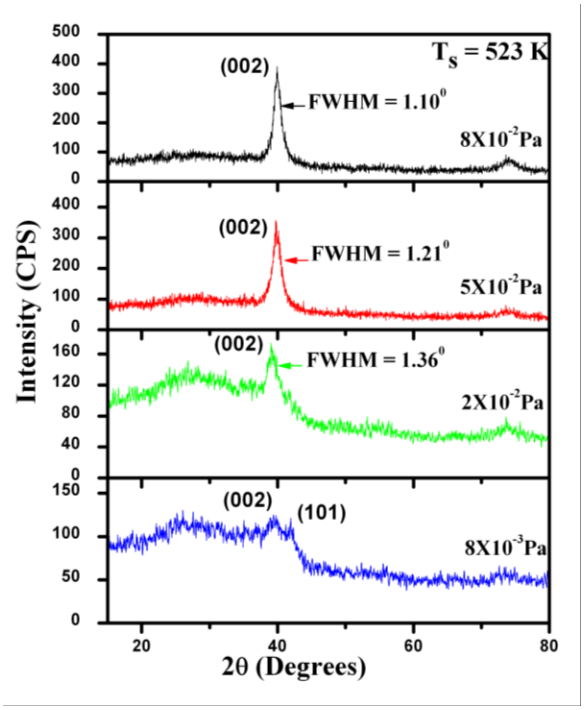

Fig. 8. XRD patterns of ZnO films formed at various oxygen partial pressures

Fig. 8 shows the XRD patterns of ZnO films deposited at various oxygen partial pressures. The films formed at oxygen partial pressure of $8x10^{-3}$ Pa consists (002), (101) phases of hexagonal ZnO. With increase of oxygen partial pressure to $8x10^{-2}$ Pa the (101) peak disappear and the intensity of (002) c-axis orientation enhanced. The intensity of the (002) phase is direct indication of the c-axis orientation perpendicular to the substrate. As the increasing of oxygen partial pressure the intensity of (002) peak increases and the peak position does not change. Schropp et al. [29] reported an increase in the preferred (002) orientation with increasing of oxygen partial pressure. Brett et al. [30] proposed a model to explain the variation in the NZO crystal structure. Which incorporated the competing effects of ion bombardment causing film amorphization and enhancement of the oxygen in the sputtering gas mixture causes better crystallinity and a preferred (002) orientation. H. Liu et al. [31] reported a sigle phase hexagonal wurtzite structure is formed in all samples, the intensity of (002) peak enhance with increase of pO_2, because of grow in oxygen rich atmosphere and the reduction of the oxygen vacancies.

The crystallite size also increased from 5.4 to 9 nm with increasing of oxygen partial pressure due to improvement of the better crystallinity of the ZnO film. The calculated crystallite size values are listed in Table 1.

Table 1. Crystallite size, deposition rate and band gap values of ZnO films vary with different oxygen partial pressures

Oxygen partial Pressure (Pa)	Deposition rate (nm)	Crystallite size (nm)	band gap (eV)
$8x10^{-3}$	5.9	5.4	3.04
$2x10^{-2}$	4.0	7.1	3.08
$5x10^{-2}$	2.7	8.0	3.10
$8x10^{-2}$	2.5	9.0	3.14

3.2.2. SEM analysis

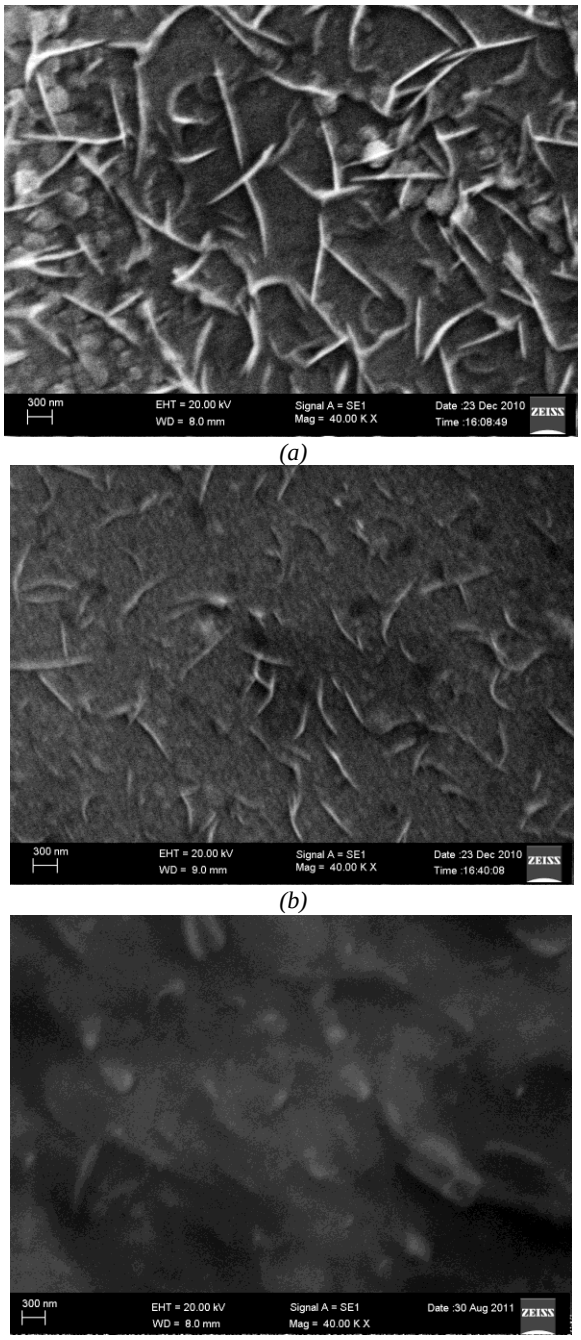

Fig. 9. SEM images of ZnO films at various oxygen partial pressures: (a) $8x10^{-3}$ Pa (b) $2x10^{-2}$ Pa (c) $5x10^{-2}$ Pa

Fig. 9 shows the scanning electron microscope images of ZnO films on silicon substrates at different oxygen partial pressures. The films deposited at oxygen partial pressure of $8x10^{-3}$ Pa the nanowires were formed parallel to the surface layer and the nanotubes were formed perpendicular to the surface of the film. As the oxygen partial pressure increased to $2x10^{-2}$ Pa the nanowires size and number decreases, and size of nanotubes were increased. On further increasing the oxygen partial pressure to $5x10^{-2}$ Pa, hexagonal cone- shape like nanorods were formed due to improvement of the (002) c-axis orientation, better crystallinity. Nakamura et al. [32] reported the hexagonal cone-shape ZnO cones achieved due to growth of (002) orientation.

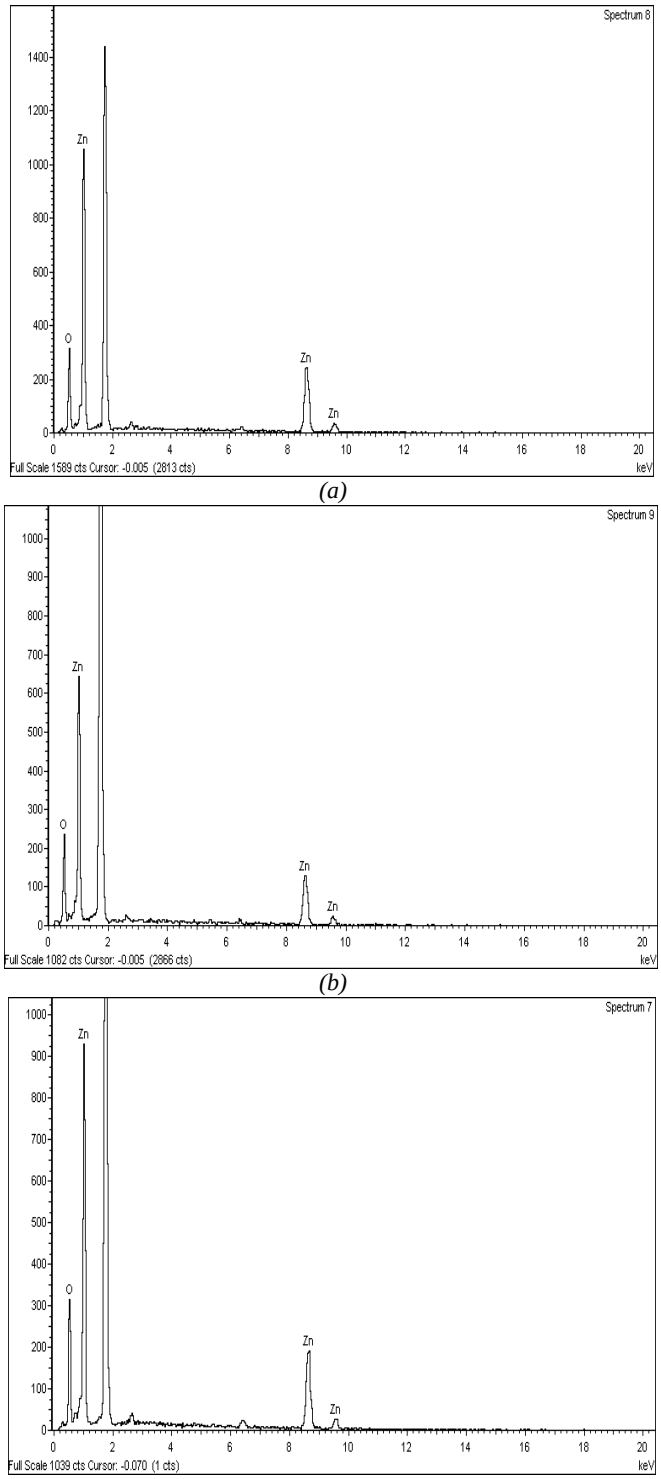

Fig. 10. EDS Spectra of ZnO films at different oxygen partial pressures: (a) 8x10-3 Pa (b) 2x10-2 Pa and (c) 5x10-2 Pa

Fig. 10 shows the EDS spectra of ZnO films at different oxygen partial pressure. The EDS spectrum reveals the Zn/O ratio decrease with increase of oxygen partial pressures because of poison of target with increase of oxygen content.

3.2.3. FTIR analysis

Fig. 11 shows Fourier transform infrared (FTIR) spectra of ZnO thin films formed at different oxygen partial pressure. FTIR spectra employed to reveal the ZnO bonding. From the FTIR spectra, the films deposited at oxygen partial pressure of $8x10^{-3}$ Pa the absorption peak located at 409 cm^{-1} corresponds to the Zn-O absorption in the hexagonal type ZnO crystal [33], and the full width at half maximum (FWHM) of absorption peak is 16 cm^{-1}.

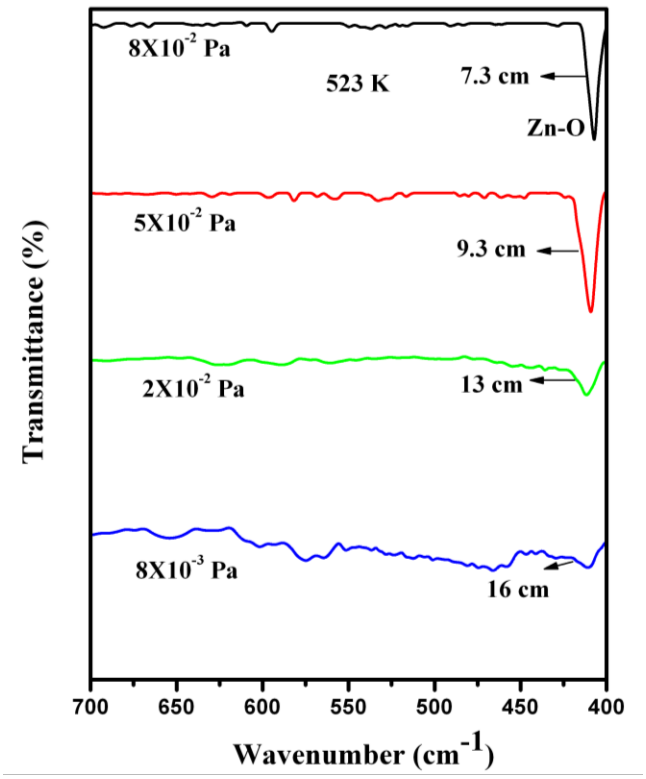

Fig. 11. FTIR spectra of ZnO films at different oxygen partial pressures

As the oxygen partial pressure increased to $8x10^{-2}$ Pa the FWHM of absorption peak decreased from 16 to 7.3 cm^{-1} due to improvement of the crystallinity of the film. The larger FWHM of absorption peak value indicates wider distribution of vibration energy of the Zn-O bonds [25].

3.2.4. Optical properties

The high optical transmittance is most useful for solar cell applications. Fig.12 shows wavelength dependence of the optical transmittance spectra of ZnO films formed at different oxygen partial pressure. The average optical transmittance of the films was 88 % in the visible region (300 – 800 nm). When the oxygen partial pressure increased from $8x10^{-3}$ to $8x10^{-2}$ Pa the optical transmittance increased due to stoichiometric of the films improved and density of defect centres decreased. The increase in transmittance of the film related to an increase in crystallite size of the (002) c-axis orientation of the film. The improvement in the transmittance of the film was due to increase of crystallite size, decrease of surface roughness and the smoother films with less grain boundaries. The sharp absorption band edge was observed at 411 nm at oxygen partial pressure of $8x10^{-3}$, it shifted towards lower wavelength side with increasing of oxygen partial pressure.

The obtained optical band gap (E_g) values of ZnO films are 3.04, 3.08, 3.10 and 3.14 eV for the oxygen partial pressure of $8x10^{-3}$, $2x10^{-2}$, $5x10^{-2}$ and $8x10^{-2}$ Pa shown in fig.13. The optical band gap of ZnO films increases with oxygen partial pressure. The optical band gap increases with oxygen partial pressure in undoped ZnO films due to oxygen vacancy is the impact factor affecting on band gap values. Oxygen vacancy is main kinds of positively charge of free carrier. Therefore oxygen vacancy can also narrow the band gap because of the Burstein- Moss effect [31]. The formation of bonds between Zn and O atoms during the deposition process the oxygen vacancy concentration is decreased as oxygen partial pressure increases resulting in the increasing of optical band gap [34]. The refractive index of ZnO films decreased from 1.96 to 1.93 with increasing of oxygen partial pressure.

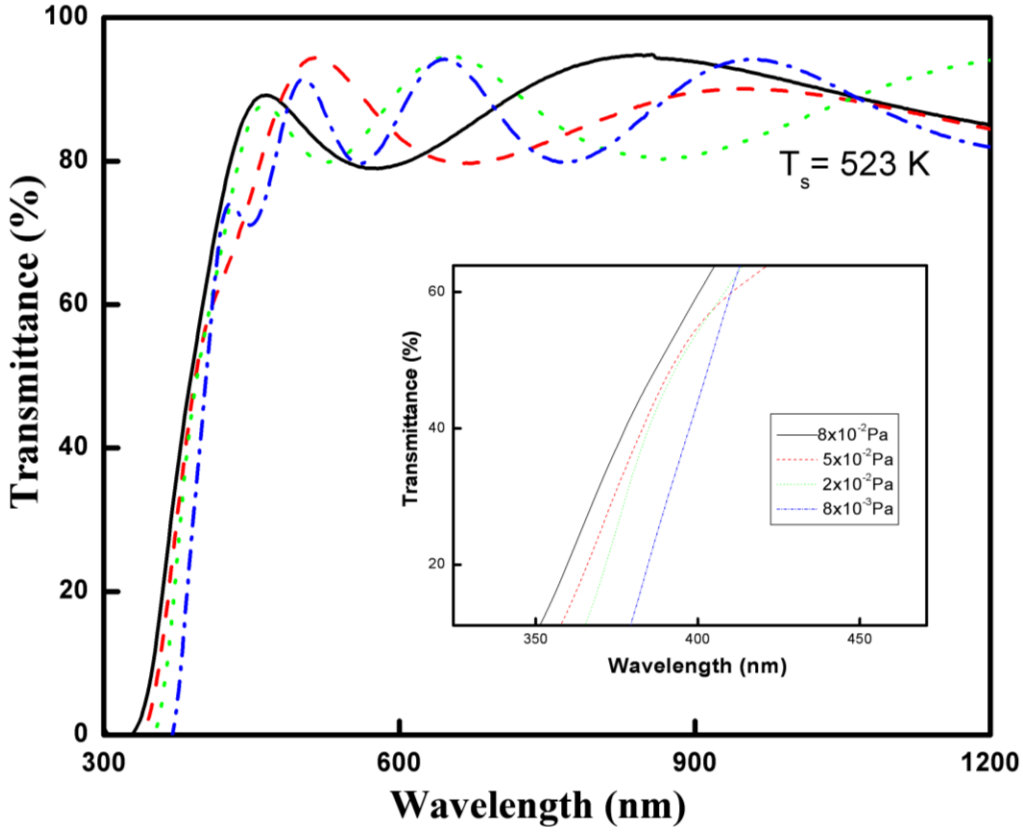

Fig. 12. Optical transmittance spectra of ZnO films at different oxygen partial pressures

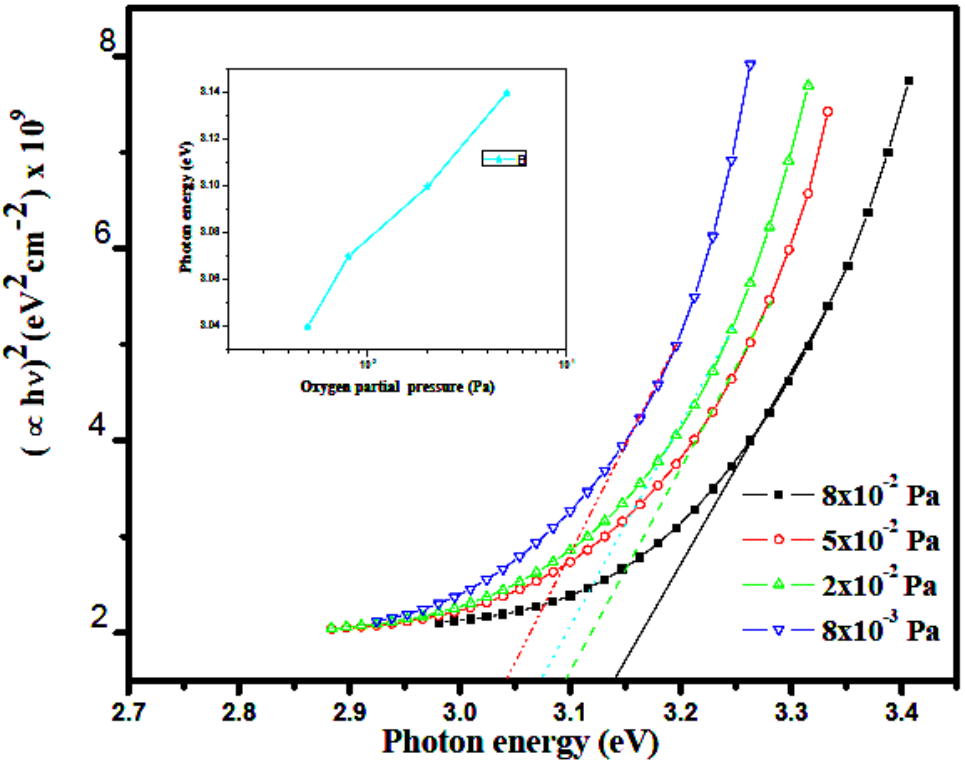

Fig. 13. Plot of (ahv)2 vs hv for ZnO films formed at different oxygen partial pressures

4. Conclusions

In this conclusion, the oxygen partial pressure and substrate temperature influenced structural, morphological and optical properties of ZnO films deposited onto p-type silicon and glass substrates by using RF magnetron sputtering systematically investigated. The films formed at oxygen partial pressure of $8x10^{-3}$ Pa consists (002), (101) phases of hexagonal ZnO. With increase of oxygen partial pressure to $8x10^{-2}$ Pa the (101) peak disappear and the intensity of (002) c-axis orientation enhanced. The SEM analysis confirms that the films formed at oxygen partial pressure of $8x10^{-3}$ Pa, the nanowires were formed parallel to the surface layer and the nanotubes were formed perpendicular to the surface of the film. ZnO nanowires are believed to be a good candidate for gas sensing applications due to its specific area, fine particle size and the quantum confinement properties Fourier transform infrared spectroscopy studies confirms the presence of Zn-O bonding at wave number of 413 cm^{-1}. The optical transmittance data reveals the average transmittance in the visible range more than 84 % for all the films. The optical band gap of ZnO films increased from 3.10 to 3.17 eV with increase of substrate temperatures 303 to 573 K.

Acknowledgements

One of the authors, Dr. S. Uthanna is thankful to the University Grants Commission, New Delhi, India for the award of UGC-BSR Faculty Fellowship.

References

[1] S. J. Kang, Y. H. Joung, Appl. Surf. Sci. **253**, 7330 (2007).
[2] W. H. Yau, P. C. Tseng, D. Lian, Nucl. Instrum. Methods Phys. Res. B **269**, 1450 (2011).
[3] C. C. Ting, C.H. Li, C. Y. Kuo, C. C. Hsu, H. C. Wang, M. H. Yang, Thin Solid Films **518**, 4156 (2010).
[4] S. H. Jeong, D. G. Yoo, D. Y. Kim, N. E. Lee, J. H. Boo, Thin Solid Films **516**, 6598 (2008).
[5] A. M. C. Ng, X. Y. Chen, F. Fang, P. W. K. Fang, H. F. Lue, C. Surya, W. K. Chen, Appl. Phys. B **100**, 851 (2010).
[6] Q. Wan, Q. H. Li, Appl. Phys. Lett. **84**, 3654 (2004).
[7] R. R. Kumar, K. Narasimha Rao, K. Rajanna, A. R. Phani, Mater. Res Bull. **52**, 167 (2014).
[8] S. Kitova, G. Danev, J. Phys: Conf. Series **223**, 012022 (2010).
[9] H. Kumarakuru, D. Cherns, A. M. Collins, Ceramic Internationals **40**, 8389 (2014).
[10] R. Anandi, R. Mohan, K. Swaminathan, K. Ravichandran, Superlatt. Microstruct. **51**, 680 (2012).
[11] A. Singh, D. Kumar, P. K. Kanna, M.Kumar, Mater. Lett. **183**, 365 (2016).
[12] C. Y. Chen, L. H. Hsiao, J. I. Chyi, J. Cryst. Growth **425**, 216 (2015).
[13] C. H. Lee, M. S. Choi, Thin Solid Films **605**, 157 (2016).
[14] L. Q. Qi, R. S. Han, L. H. Liu, H. Y. Sun, Ceramic Internationals **42**, 18925 (2016).
[15] S. Hamrit, K. Djessas, N. Brihi, B. Viallet, K. Medjnoun, S. E. Grillo, Ceramic International **42**, 16212 (2016).
[16] T. K. Subramanyam, B. Srinivasulu Naidu, S. Uthanna, Opt. Mater. **13**, 239 (1999).
[17] S. Sigh, R. S. Srinivasa, S. S. Major, Thin Solid Films **515**, 8718 (2007).
[18] R. Kumar, N. Khare, V. Kumar, G. L. Bhatta, Appl. Surf. Sci. **254**, 6509 (2008).
[19] B. D. Cullity, Elements of X-ray Diffraction, second ed., Addison Wesley, London, 1978.
[20] S. Lalita, R. Sathyamurthy, S. Senthilarasu, A. Subbarayan, K. Natarajan, Sol. Energy Mater. Sol. Cells **82**, 187 (2004).
[21] L. P. Pong, L. Fong, X. F. Yang, H. B. Ruan, Y. J. Li, Q. L. Huang, C. Y. Kong, Physica E **41**, 1819 (2009).
[22] C. C. Wu, D. S. Wuu, P. R. Lin, T. N. Chen, R. H. Horns, Nano Scale Res. Lett. **4**, 377 (2009).
[23] S. J. Kung, Y. H. Joung, Appl. Surf. Sci. **253**, 7330 (2007).
[24] Y. Zhao, Y. Jiang and Y. Fang, J. Cryst. Growth **307**, 278 (2007).
[25] D. C. Agarwal, R. S. Chauhan, D. Kabiraj, F. Singh, S. A. Khan, D. K. Avasthi, J. Appl Phys. **99**, 123105 (2006).
[26] F. Chaabouni, M. Abaab, B. Rezig, Mater. Sci. Eng. B **109**, 236 (2004).
[27] P. Zhou, H. Liu, L. Zhang, X. Suo, Z. Liang, Y. Liu, Y. Li, Z. Jiangg, Z. Wang, J. Mater. Sci: Mater Electron **27**, 7822 (2016).
[28] R. Swanepoel, J. Phys. E: Sci. Instrum. **16**, 1214 (1983).
[29] R. E. I. Schropp, A. Madan, J. Appl Phys. **66**, 2020 (1989).
[30] M. J. Brett, R. R. Parsons, J. Mater. Sci. **22**, 3611 (1987).
[31] H. Liu, P. Zhou, L. Zhang, Z. Liang, H. Zhao, Z. Wang, Materials Letters **164**, 509 (2016).
[32] Nakamura, K. Okazak, I. A. Palani, M. Higashihata, T. Okada, Appl. Phys. A **103**, 959 (2011).
[33] P. K. Kannan, R. Saraswathi, J. Bosco, B. Rayappan, Sens. Actuators A **164**, 8 (2010).
[34] M. G. Tsoutsouva, C. N. Panagopoulos, D. Papadimitrior, I. Fasaki, M. Ompitsas, Mater. Sci. Eng. B **176**, 480 (2011).

*Corresponding author: sbbreddy82@gmail.com